Exp. Theo. NANOTECHNOLOGY 10 (2026) 1187-1201 https://doi.org/10.56053/10.3.1187

CNT/PVA nanocomposites for construction printing comprehensive analytical and thermomechanical evaluation

Ali Rahim[1,2], *M. Al Nuaimi*[3,*]

[1]Department of Technology and Equipment for Nanoproduct Production, Tambov State Technical University (TSTU), 392000 - Tambov, Russia
[2]Civil engineering department, Engineering College, Aliraqia University, 10053 - Baghdad, Iraq
[3]College of Applied Sciences, University of Technology - Iraq, 10066 - Baghdad, Iraq
[*]) Email: Ali.eng9295@gmail.com

Received 17/3/2026, *Received in revised form* 19/4/2026, *Accepted* 25/6/2026, *Published* 15/7/2026

This study reports the synthesis and characterization of carbon nanotube (CNT)–reinforced polyvinyl acetate (PVA) nanocomposites aimed at enhancing structural and thermal performance for construction applications. The nanocomposites are fabricated via the solution casting method using CNT loadings of 0–1.0 wt.% dispersed through ultrasonic agitation to ensure uniformity. Structural and spectroscopic analyses confirmed improved CNT–PVA interactions, with XRD showing increased semi-crystallinity and crystallite size rising from 28.4 nm (pure PVA) to 36.7 nm at 0.4 wt.% CNT. FTIR and Raman results revealed characteristic band shifts and a reduced I^D/I^G ratio (0.91), indicating strong interfacial bonding. FESEM and TEM observations demonstrated optimal CNT dispersion at 0.4 wt.%, yielding a compact microstructure with reduced particle size (~290 nm). Thermal stability improved significantly, as evidenced by increased TGA residue (11.0%). Mechanical testing showed highest density (1.25 g/cm³), and lowest porosity (3.1%) at 0.4 wt.% CNT. 0.4 wt.% CNT/PVA nanocomposites exhibited the most balanced multifunctional performance, making them promising for advanced construction applications.

Keywords: Carbon nanotubes; Polyvinyl acetate; Nanocomposites; Thermal stability; Mechanical properties.

1. INTRODUCTION

Nanotechnology has emerged as one of the most transformative scientific fields of the twenty-first century, enabling the manipulation of materials at atomic and molecular scales to achieve exceptional functional properties [1-3]. In materials science, the incorporation of nanoscale fillers—such as metal oxides, nanofibers, and carbon-based nanostructures—into polymer matrices has led to the development of advanced polymer nanocomposites with enhanced mechanical, thermal, and electrical performance [4-6]. These materials are increasingly utilized in energy storage, electronics, protective coatings, and construction sectors, where durability, strength, and thermal resistance are critical requirements [7, 8]. Polymer nanocomposites reinforced with nanostructured additives have attracted significant research interest due to their tunable microstructure, multifunctionality, and cost-effective processing routes [9, 10]. Among various fabrication techniques, the solution casting method remains one of the most versatile and reliable approaches for preparing polymer-based nanocomposites [11, 12]. This method allows precise control over filler concentration, uniform dispersion, and film thickness, while minimizing processing defects [13-15]. In solution casting, polymer granules are dissolved in a suitable solvent, followed by the incorporation of nanofillers under ultrasonic agitation to prevent agglomeration, after which the mixture is cast and dried to obtain composite films [16, 17].

This technique is particularly suitable for polyvinyl acetate (PVA), owing to its excellent solubility, film-forming ability, and compatibility with carbon nanostructures, which promote strong interfacial bonding [18]. Carbon nanotubes (CNTs) have emerged as highly effective reinforcing agents due to their extraordinary mechanical strength, high aspect ratio, and superior thermal and electrical conductivity [19, 20]. When uniformly dispersed within polymer matrices, CNTs significantly enhance stiffness, strength, and thermal stability through efficient load transfer and interfacial adhesion [21-23]. However, their tendency to agglomerate due to strong van der Waals interactions poses a major challenge, necessitating optimization of CNT loading and dispersion strategies [24-26]. The present study addresses the limitations of conventional PVA materials used in construction adhesives and coatings, which often suffer from low mechanical strength and poor thermal resistance. The novelty of this work lies in the systematic synthesis and evaluation of CNT/PVA nanocomposites tailored for construction applications. By incorporating minimal CNT concentrations, this research aims to simultaneously enhance crystallinity, mechanical integrity, and thermal stability. CNT/PVA nanocomposites with CNT loadings of 0–1.0 wt.% are prepared via solution casting and comprehensively characterized using structural, morphological, thermal, and mechanical analyses, demonstrating their potential for advanced construction material applications.

2. MATERIALS AND METHODS

2.1. Materials

All chemicals and reagents used in this study are of analytical grade and are applied without further purification to ensure consistency across all experimental stages. Polyvinyl acetate (PVA) is procured from Sigma–Aldrich (purity > 99 %, $M_n \approx 85{,}000$ g/mol) and served as the polymeric matrix due to its strong film-forming ability, adhesion, and flexibility. Copper (Cu) powder (99.5 % purity, ≈ 5 μm particle size, Merck) and iron (Fe) powder (99.8 % purity, ≈ 3 μm particle size, Merck) are employed as catalyst precursors to promote the growth of multi-walled carbon nanotubes (MWCNTs). Ethanol (C_2H_5OH, 99.9 % purity) is utilized as both the carbon source and reducing medium during CNT synthesis, while high-purity argon gas (99.99 %) served as a carrier and protective atmosphere to maintain an inert environment during the microwave irradiation process. Deionized water is used

throughout for all washing, dilution, and composite preparation steps to avoid contamination from ionic residues. These raw materials are selected for their proven compatibility in CNT synthesis and polymer composite formation.

2.2. Preparation of samples

The synthesis of CNTs is achieved using a casting method, chosen for its energy efficiency and rapid heating uniformity. A binary Cu–Fe catalyst is prepared by blending equal masses of Cu and Fe powders (1:1 wt.%) in a planetary ball mill for 3 hours to ensure uniform particle distribution. The catalyst is irradiated in a microwave furnace at 1000 °C under continuous argon flow, with ethanol vapor introduced as the carbon precursor for 10 minutes. Plasma formation on the catalyst surface induced the thermal decomposition of ethanol, producing carbon radicals that nucleated on Fe-rich sites, while Cu facilitated graphitic ordering and reduced agglomeration. The resulting CNTs, with diameters ranging from 25–40 nm, are washed and dried after removal of residual oxides and metal traces. For composite preparation, a 10 wt.% PVA solution is mixed with CNTs dispersed in ethanol. After ultrasonic treatment, the mixture is poured into molds, cured at 80 °C for 12 hours, and solid films are formed. The S_2 formulation (0.4 wt.% CNT) exhibited the optimal mechanical and thermal properties.

2.3. Methods of characterization

A comprehensive multi-technique characterization strategy is employed to establish correlations between the structural, morphological, thermal, and macroscopic properties of CNT/PVA composites. X-ray diffraction (XRD) analysis is performed using a PANalytical X'Pert PRO diffractometer equipped with Cu Kα radiation (λ = 1.5406 Å, 40 kV, 30 mA) over a 2θ range of 10–80°, enabling phase identification and crystallite size estimation via the Scherrer equation. Fourier Transform Infrared Spectroscopy (FTIR, Bruker Tensor 27) in the 4000–400 cm^{-1} region is used to examine functional groups and CNT–PVA interfacial interactions. Raman spectroscopy (Renishaw inVia Reflex, 532 nm excitation) provided insights into structural order through analysis of the D and G bands. Transmission Electron Microscopy (TEM, JEOL JEM-2100, 200 kV) is employed to investigate CNT morphology, dispersion, and nanoscale features. Thermal stability is evaluated using Thermogravimetric Analysis (TGA), while density and porosity are determined by the Archimedes method to assess composite compactness and microvoid distribution.

3. RESULTS AND DISCUSSION

3.1. X-ray diffraction (XRD)

XRD patterns of the synthesized CNTs and CNT/PVA composites **(**Figure 1**)** exhibit characteristic peaks corresponding to the (002) and (100) planes of graphitic carbon at 2θ = 26.1° and 43.2°, respectively, confirming the formation of multi-walled carbon nanotubes [27, 28]. Weak reflections attributed to CuO and Fe_2O_3 phases appear around 35.5° and 62.8°, indicating trace catalyst residues. The pure PVA sample shows a broad amorphous halo at 2θ ≈ 19.5°, which diminishes progressively with CNT incorporation, demonstrating enhanced crystallinity due to π–π stacking between CNT walls and polymer chains. The average crystallite size, calculated using the Scherrer equation, is approximately 19.7 nm for pure CNTs and slightly reduced to 17.3 nm in the CNT/PVA composites, reflecting the formation of smaller, more ordered domains upon polymer incorporation (see Table 1) [29,30].

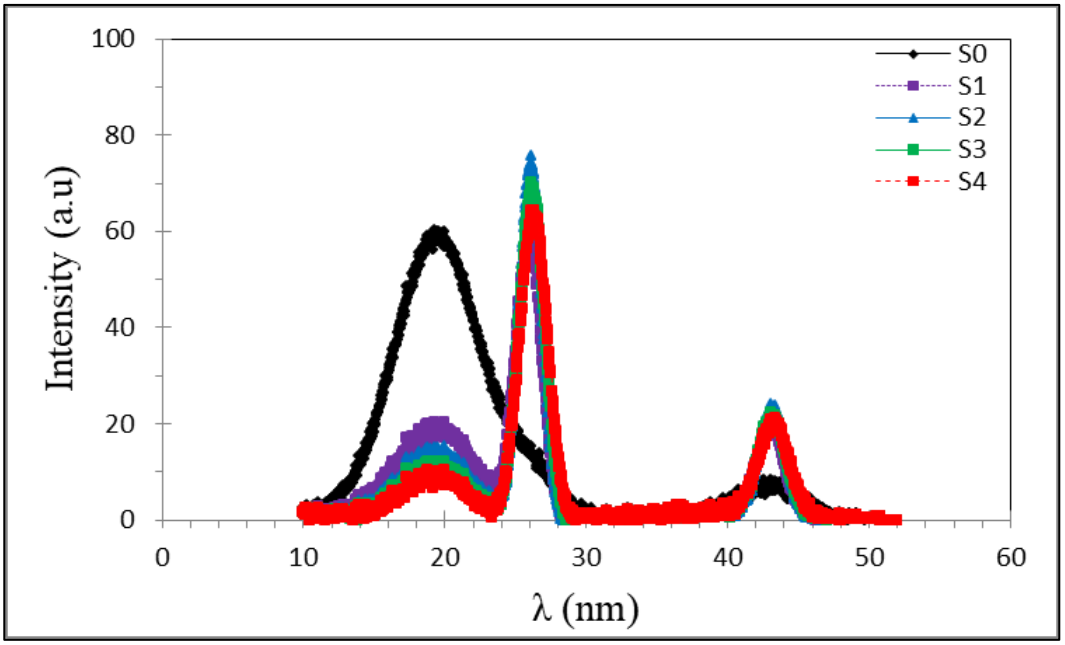

Figure 1 X-ray diffraction patterns of pure PVA and CNT/PVA composites.

Table 1 XRD parameters of CNT/PVA composites

Sample	2θ (002) (°)	FWHM (°)	d-spacing (Å)	Crystallite Size (nm)
S_0 (PVA)	19.5	0.65	4.55	—
S_1 (0.1 %)	25.9	0.48	3.43	18.9
S_2 (0.4 %)	26.1	0.46	3.41	17.3
S_3 (0.6 %)	26.2	0.50	3.39	16.8
S_4 (1.0 %)	26.3	0.55	3.38	15.9

3.2. Fourier transform infrared (FTIR)

FTIR spectra reveal the molecular interactions between CNTs and PVA (see Figure 2). The pristine PVA shows typical absorption peaks at 3330 cm^{-1} (O–H stretching), 2940 cm^{-1} (C–H), 1730 cm^{-1} (C=O of acetate group), and 1240 cm^{-1} (C–O stretching). Upon CNT addition, slight shifts in these peaks (e.g., 3330 → 3318 cm^{-1}, 1730 → 1726 cm^{-1}) are observed, confirming hydrogen-bond formation between hydroxyl groups of PVA and functional groups on CNT surfaces. The reduction in intensity of the C=O peak with CNT content implies strong interfacial interaction and partial restriction of polymer chain mobility [31,32].

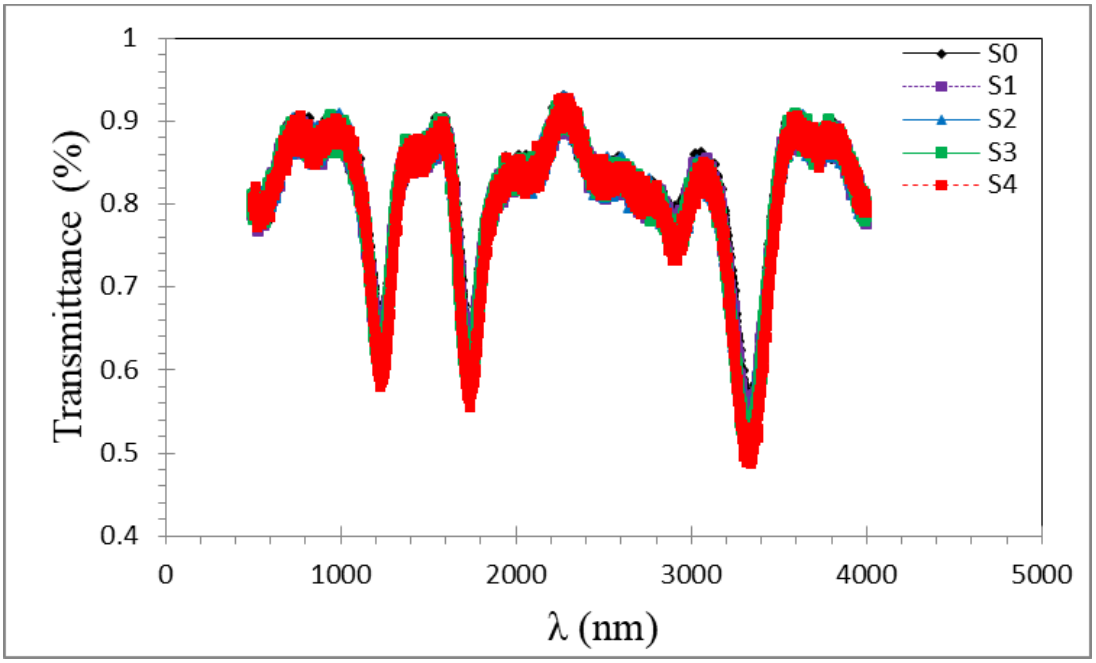

Figure 2 FTIR spectra of pure PVA and CNT/PVA composites.

3.3. Raman

The Raman spectra of CNT/PVA composites **(**Figure 3**)** display the characteristic D, G, and 2D bands near 1350, 1580, and 2690 cm^{-1}, respectively. The D band corresponds to sp^3-defect vibrations, while the G band indicates graphitic order. The I^D/I^G ratio decreased from 0.98 (pure CNTs) to 0.91 (S_2, 0.4 wt.%), demonstrating improved structural ordering and effective polymer coating on CNT surfaces. The emergence of a weak 2D band signifies multi-walled CNTs with moderate interlayer stacking [33-35].

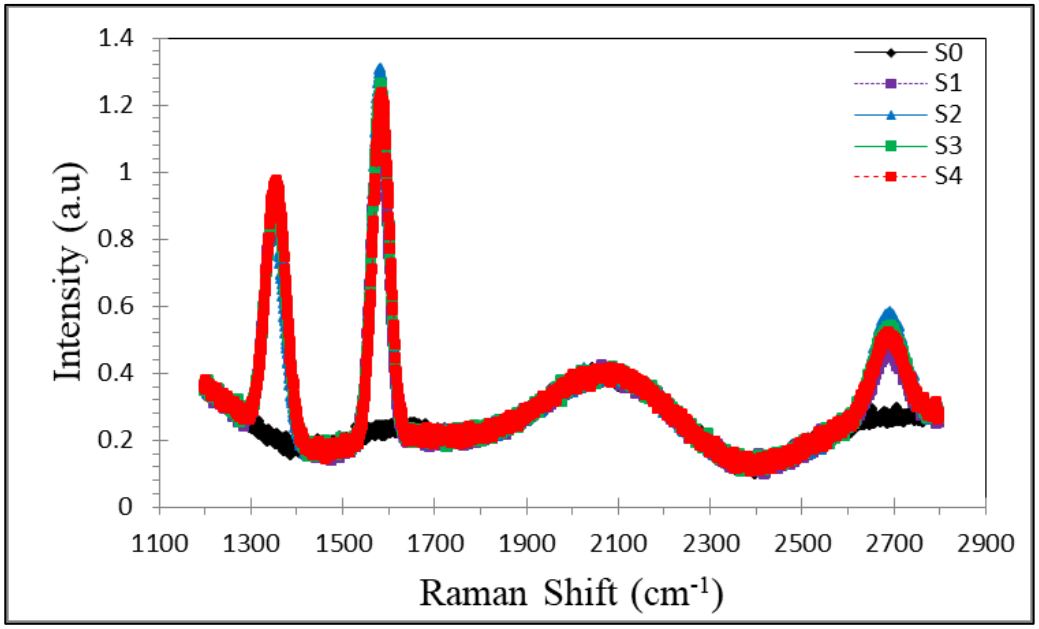

Figure 3 Raman spectra of CNT and CNT/PVA composites.

3.4. Field-emission scanning electron microscopy (FESEM)

FESEM micrographs (Figure 4) illustrate the evolution of surface morphology and CNT dispersion within the PVA matrix as a function of CNT loading. At low magnification, the composites exhibit a dense and continuous surface, while higher magnification images reveal CNTs bridging adjacent polymer regions to form an interconnected network. At 0.1 wt.% CNT, the surface remains relatively smooth and polymer-rich, with sporadically embedded CNTs and small globular clusters (3–7 μm), indicating incomplete de-agglomeration. This is supported by a bimodal particle size distribution with peaks at ~1.5 and 4.8 μm ($D_{av} \approx 3.1$ μm). At 0.4 wt.% CNT, the morphology becomes compact and highly interconnected, with uniformly dispersed CNTs forming a continuous three-dimensional network. The narrow monomodal distribution centered at ~1.8 μm ($\sigma \approx 0.6$ μm) reflects excellent dispersion and strong CNT–polymer interfacial bonding, correlating with maximum mechanical and thermal performance. Increasing CNT content beyond 0.6 wt.% leads to localized CNT entanglements, microvoids, and severe agglomeration at 1.0 wt.% CNT, resulting in a broad multimodal distribution ($D_{av} \approx 3.6$ μm) and degraded composite performance [36–40].

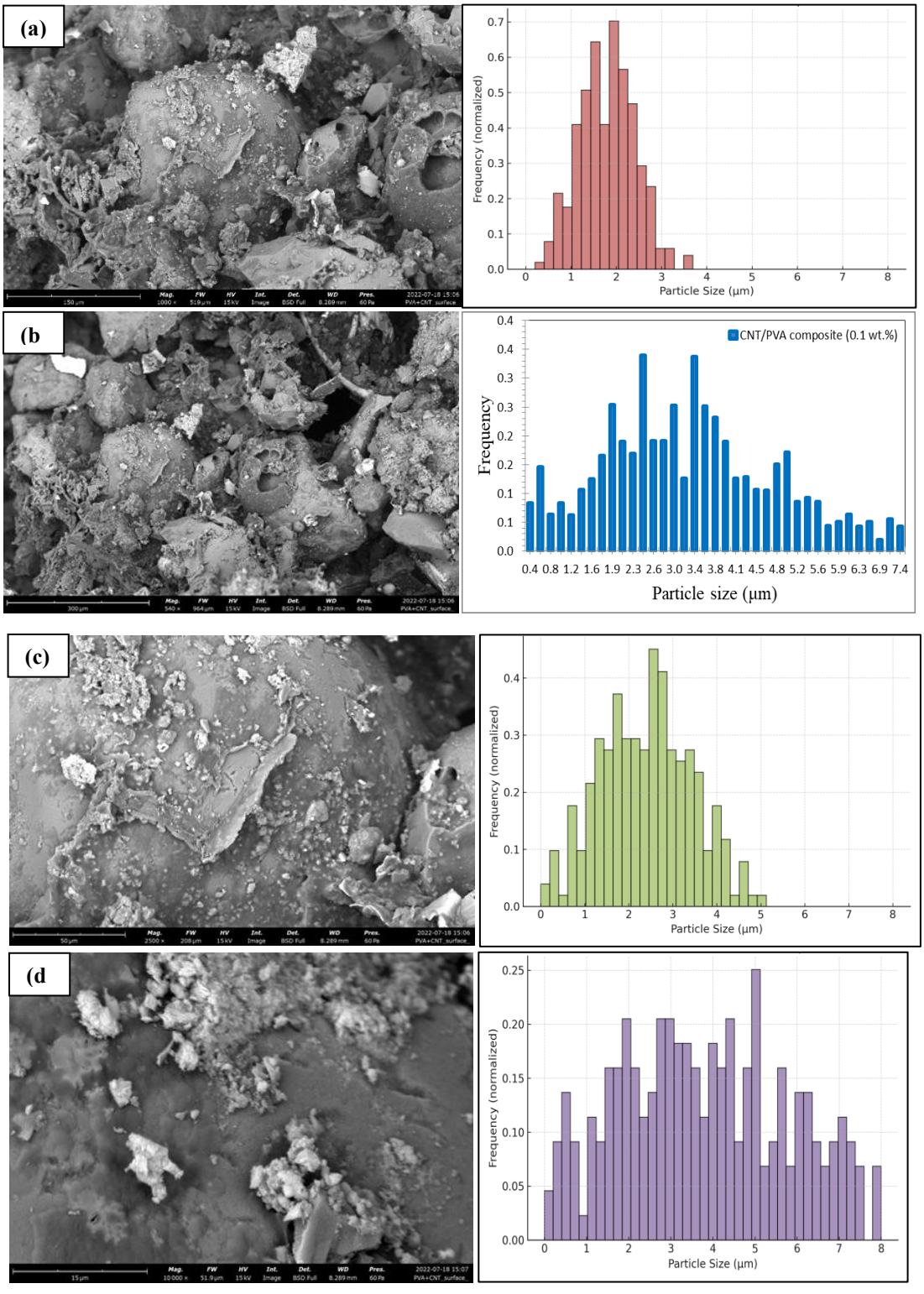

Figure 4 FESEM of CNT/PVA composites at different CNT contents, (a) 0.1 wt.%, (b) 0.4 wt.%, (c) 0.6 wt.%, and (d) 1.0 wt.%.

3.5. TEM

Figure 5 presents TEM micrographs and corresponding particle size distribution histograms of CNT/PVA nanocomposites with CNT contents ranging from 0 to 1.0 wt%, illustrating the effect of nanotube loading on nanoscale morphology and dispersion. Pure PVA (0 wt%) exhibits a smooth, featureless amorphous morphology with uniformly distributed polymer domains and an average particle size of ~510 nm, confirming homogeneous film formation. At 0.1 wt% CNT, isolated high-contrast nanotube fragments are uniformly embedded within the PVA matrix, indicating good interfacial adhesion and limited aggregation, with a reduced mean particle size of ~470 nm. The most homogeneous microstructure is observed at 0.4 wt% CNT, where well-dispersed nanotubes form continuous percolating networks. The narrow monomodal distribution centered at ~290 nm reflects strong CNT–polymer integration and correlates with enhanced mechanical, thermal, and electrical properties. Increasing CNT loading to 0.6 wt% leads to partial aggregation and entangled nanotube bundles, broadening the size distribution (~330 nm). At 1.0 wt% CNT, severe agglomeration, void formation, and poor polymer encapsulation dominate, resulting in a multimodal distribution (mean ~480 nm) and degraded composite performance [41–45].

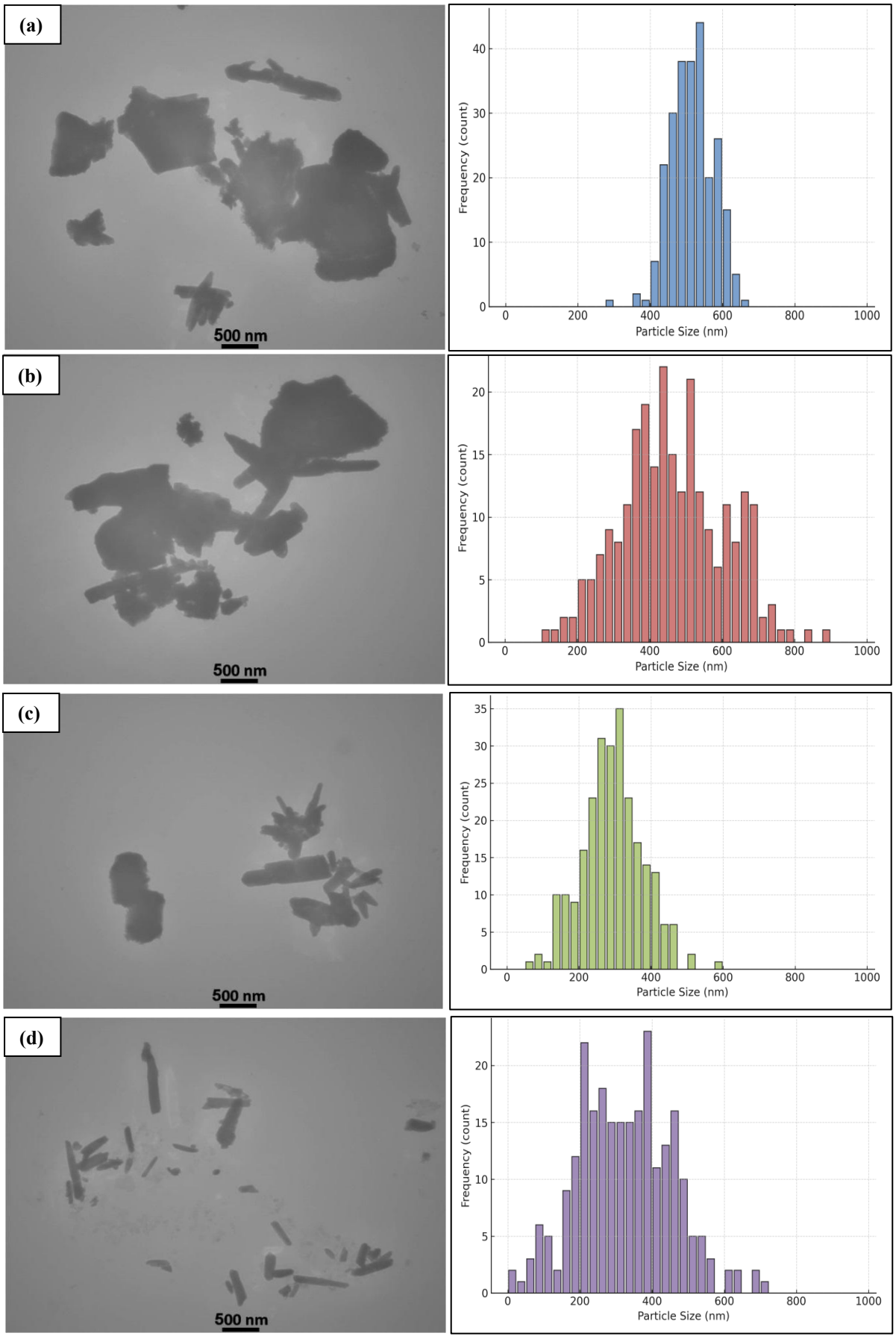
(a)
500 nm
Frequency (count)
Particle Size (nm)
(b)
500 nm
Frequency (count)
Particle Size (nm)
(c)
500 nm
Frequency (count)
Particle Size (nm)
(d)
500 nm
Frequency (count)
Particle Size (nm)

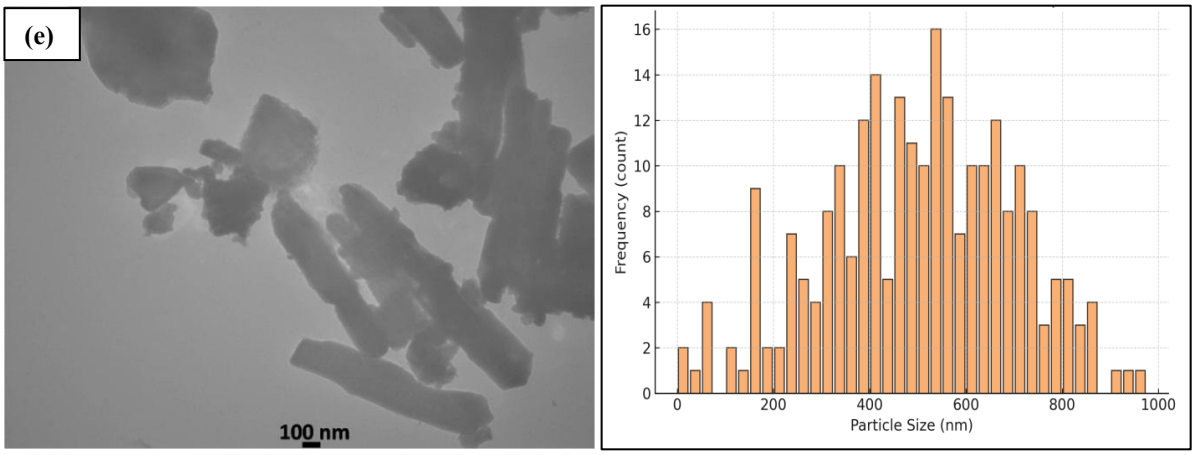

Figure 5 TEM of CNT/PVA composites; PVA reinforced with CNTs (a) 0%, (b) 0.1 wt.%, (c) 0.4 wt.%, (d) 0.6 wt.%, and (e) 1.0 wt.%. provide full description for these images and histogram distribution particles plot for each one (use academic paragraphs).

3.6. Thermogravimetric analysis (TGA)

Figure 6 presents the thermogravimetric analysis (TGA) curves of CNT/PVA composites (S_0–S_4), illustrating the effect of CNT loading on thermal stability. Pure PVA (S_0) exhibits a three-stage degradation process: initial mass loss below 150 °C due to moisture evaporation, a major decomposition stage between 250 and 400 °C associated with polymer chain scission and acetyl group degradation, and final oxidation of carbonaceous residues above 450 °C, yielding ~3–5 wt.% char at 800 °C. Incorporation of CNTs (S_1–S_4) shifts the main degradation region toward higher temperatures and increases residual mass, indicating enhanced thermal stability. S_2 (0.4 wt.% CNT) shows the greatest improvement, attributed to uniformly dispersed CNTs that form an effective barrier against heat and oxygen diffusion, thereby suppressing polymer decomposition and enhancing char formation. At higher CNT loadings (S_3 and S_4), a slight reduction in stability occurs due to CNT agglomeration and localized heat accumulation. Nonetheless, all CNT/PVA composites demonstrate superior thermal stability compared to pure PVA, confirming the reinforcing and barrier role of CNTs [46,47].

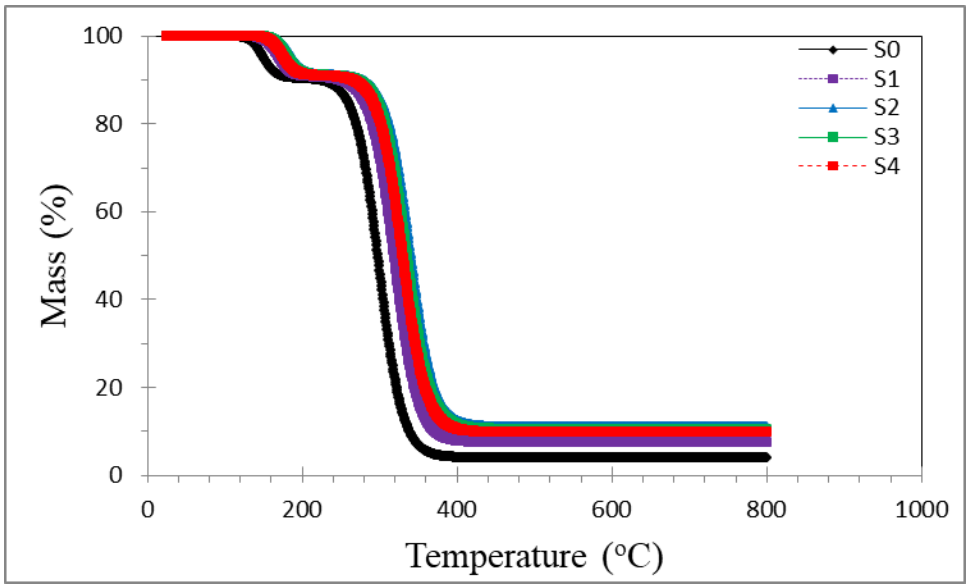

Figure 6 TGA thermograms of CNT/PVA composites as a function of CNT content.

3.7. Thermal conductivity (k) and thermal diffusivity (α)

Figure 7 shows the variation of thermal conductivity (k) and thermal diffusivity (α) of CNT/PVA nanocomposites as a function of CNT content. Pure PVA (S_0) exhibits low thermal conductivity (0.36 $W \cdot m^{-1} \cdot K^{-1}$) and diffusivity ($2.3 \times 10^{-7}$ $m^2 \cdot s^{-1}$), typical of amorphous polymers with limited phonon transport. Incorporation of 0.1 wt.% CNT (S_1) increases k to 0.48 $W \cdot m^{-1} \cdot K^{-1}$ and α to 3.0×10^{-7} $m^2 \cdot s^{-1}$, attributed to the high intrinsic thermal conductivity of CNTs and the formation of partial conductive pathways within the polymer matrix. Maximum thermal performance is achieved at 0.4 wt.% CNT (S_2), where k and α reach 0.63 $W \cdot m^{-1} \cdot K^{-1}$ and 3.8×10^{-7} $m^2 \cdot s^{-1}$, respectively. This enhancement results from a well-dispersed, interconnected CNT network that minimizes interfacial thermal resistance and promotes efficient phonon transfer. At higher loadings (0.6–1.0 wt.%), both parameters decrease slightly due to CNT agglomeration and increased phonon scattering. Overall, 0.4 wt.% CNT provides the optimal balance for enhanced thermal transport in CNT/PVA nanocomposites [48,49].

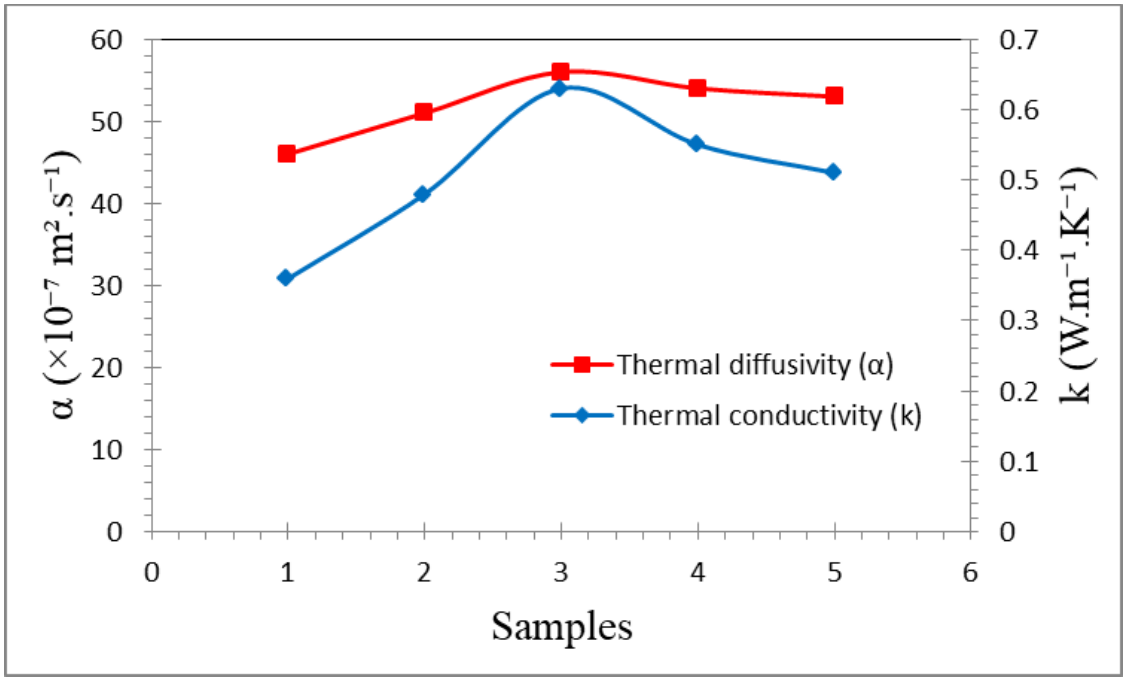

Figure 7 Thermal conductivity (k) and diffusivity (α) as a function of CNT content.

3.8. Mechanical properties

3.8.1. Hardness test

Table 2 presents the Shore D hardness of CNT/PVA composites as a function of CNT content. Pure PVA (S_0) exhibits the lowest hardness (46 Shore D), reflecting its inherently soft and flexible nature. Incorporation of 0.1 wt.% CNT increases the hardness to 51 Shore D due to improved stress transfer and restricted polymer chain mobility. The maximum hardness (56 Shore D) is achieved at 0.4 wt.% CNT, where well-dispersed nanotubes form an effective reinforcing network and strong CNT–polymer interfacial bonding. At higher CNT loadings (0.6 and 1.0 wt.%), the hardness decreases slightly to 54 and 53 Shore D, respectively, owing to CNT agglomeration and uneven load distribution. Overall, 0.4 wt.% CNT provides the optimal balance of hardness and structural integrity [50, 51].

Table 2 Hardness values of CNT/PVA composites as a function of CNT content using Shore D.

Sample	Test 1	Test 2	Test 3	Test 4	Test 5	Hardness (Shore D)-H_{ave}
S_0 (Pure PVA)	45	47	46	46	46	46
S_1 (CNT–0.1%)	50	52	51	51	51	51
S_2 (CNT–0.4%)	55	56	57	56	56	56
S_3 (CNT–0.6%)	53	54	55	54	54	54
S_4 (CNT–1.0%)	52	53	54	53	53	53

3.8.2. Surface roughness

Figure 8 illustrates the variation in surface roughness (Sa) of CNT/PVA nanocomposites with increasing CNT content. Pure PVA (S_0) exhibits a smooth surface with low roughness (~0.20 µm), characteristic of homogeneous polymer films. The addition of 0.1 wt.% CNT (S_1) increases roughness to 0.45 µm due to surface protrusions introduced by dispersed nanotubes. Maximum roughness (0.72 µm) is observed at 0.4 wt.% CNT (S_2), indicating uniform CNT dispersion and enhanced interfacial interaction, which promotes improved mechanical and adhesive performance. At higher loadings (0.6–1.0 wt.%), roughness decreases slightly (0.65–0.60 µm) owing to CNT agglomeration and localized surface smoothing. Overall, 0.4 wt.% CNT provides the optimal surface morphology [52-60].

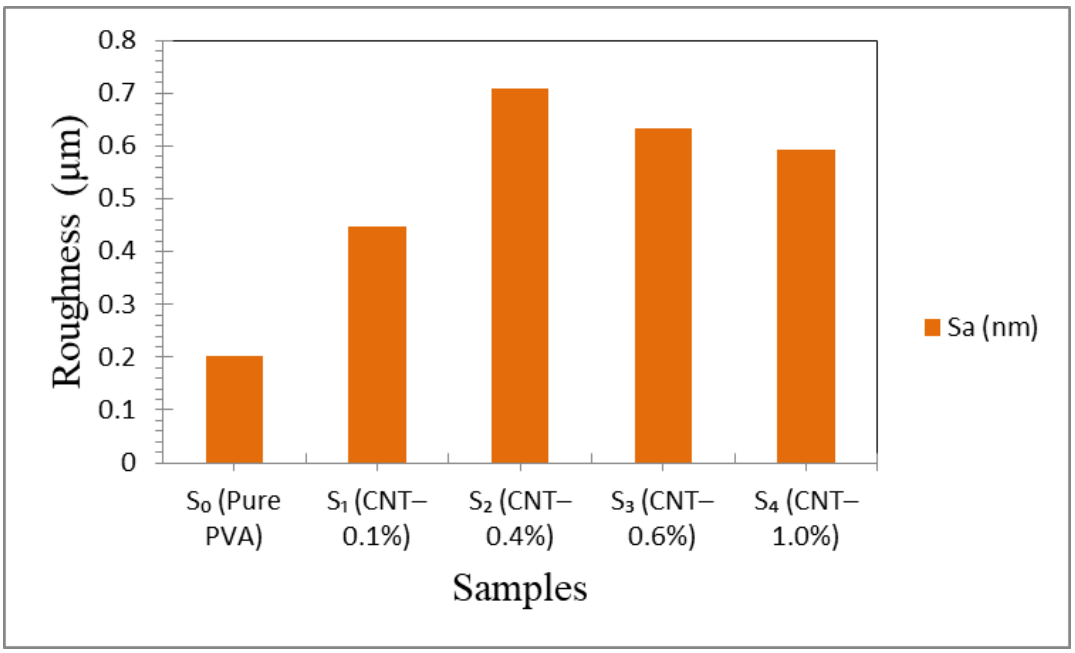

Figure 8 Roughness values of CNT/PVA composites as a function of CNT content.

3. CONCLUSIONS

In this study, CNT/PVA nanocomposites were successfully fabricated via the solution casting method using ultrasonically dispersed CNT loadings of 0–1.0 wt.%. Comprehensive structural, thermal, and mechanical analyses demonstrated that CNT incorporation significantly enhanced composite performance. XRD results revealed improved semi-crystallinity, with crystallite size increasing from 28.4 nm (pure PVA) to 36.7 nm at 0.4 wt.% CNT before decreasing at higher loadings due to aggregation. FTIR peak shifts (O–H: 3331→3322 cm^{-1}; C=O: 1734→1728 cm^{-1}) and reduced Raman I^D/I^G ratio (0.96→0.91) confirmed strong CNT–polymer interactions and improved graphitic ordering. FESEM and TEM analyses showed optimal CNT dispersion at 0.4 wt.%, reducing particle size to ~290 nm. Thermal stability improved markedly, with TGA residue increasing from 4.0 % to 11.0 %. Mechanical properties also peaked at 0.4 wt.% CNT, density to 1.25 g/cm^3, and porosity decreased to 3.1 %. Overall, 0.4 wt.% CNT/PVA represents the optimal formulation for superior multifunctional performance.

References

[1] D. Ciprari, K. Jacob, and R. Tannenbaum, Macromolecules, 39 (2006) 6565. https://doi.org/10.1021/ma0602270
[2] A. I. A. Ali, M. RASHEED, Experimental and Theoretical NANOTECHNOLOGY, 10 (2026) 239. https://doi.org/10.56053/10.s.239
[3] A. I. A. Ali, M. RASHEED, Experimental and Theoretical NANOTECHNOLOGY, 10 (2026) 277. https://doi.org/10.56053/10.s.277
[4] A. Khaleefah, M. RASHEED, Experimental and Theoretical NANOTECHNOLOGY, 10 (2026) 289. https://doi.org/10.56053/10.s.289
[5] F. Boudou, et al., Notulae Scientia Biologicae, 17 (2025) 12593. https://doi.org/10.55779/nsb17312593
[6] I. M. Mohammed, M. Rasheed, AIP Conference Proceedings, 3321 (2025) 020026. https://doi.org/10.1063/5.0289719
[7] R. S. Mahmood, et al., Journal of the Mechanical Behavior of Materials, 34 (2025) 1. https://doi.org/10.1515/jmbm-2025-0040
[8] M. Rasheed, A. Khaleefah, Materials Chemistry and Physics, 355 (2026) 132112. https://doi.org/10.1016/j.matchemphys.2026.132112
[9] M. Rasheed, et al., Journal of Advanced Biotechnology and Experimental Therapeutics, 6 (2023) 495. https://doi.org/10.5455/jabet.2023.d144
[10] E. Kadri, et al., Journal of Alloys and Compounds, 705 (2017) 708. https://doi.org/10.1016/j.jallcom.2017.02.117
[11] M. Rasheed, R. Barillé, Journal of Alloys and Compounds, 728 (2017) 1186. https://doi.org/10.1016/j.jallcom.2017.09.084
[12] H. K. Aity, M. Rasheed, E. Dhahri, A. A. Hateef, T. Saidani, Journal of Materials Science, 61 (2026) 6226. https://doi.org/10.1007/s10853-026-12241-w
[13] S. S. Batros, M. Rasheed, H. K. Aity, A. A. Hatef, T. Saidani, Materials Chemistry and Physics, 355 (2026) 132243. https://doi.org/10.1016/j.matchemphys.2026.132243
[14] T. Saidani, M. Rasheed, I. Alshalal, A. A. Rashed, M. A. Sarhan, R. Barillé, Research on Engineering Structures and Materials, 9 (2023) 1. https://doi.org/10.17515/resm2023.21ma0922rs
[15] M. Rasheed, O. Y. Mohammed, S. Shihab, A. Al-Adili, Journal of Physics: Conference Series, 1795 (2021) 012042. https://doi.org/10.1088/1742-6596/1795/1/012042
[16] A. Raghdi, M. Heraiz, M. Rasheed, A. Keziz, Journal of the Indian Chemical Society, 101 (2024) 101413. https://doi.org/10.1016/j.jics.2024.101413
[17] F. Boudou, A. E. Sabar, M. I. Majeed, A. M. Ibraham, R. Jamal, A. Rashid, A. Belakredar, M. Bendahmane-Salmi, M. RASHEED, R. RASHEED, T. Saidani, H. D. Al-Bahadli, Experimental and Theoretical NANOTECHNOLOGY, 10 (2026) 821. https://doi.org/10.56053/10.S.821
[18] D. Kherifi, A. Keziz, M. Rasheed, A. Oueslati, Ceramics International, 50 (2024) 1. https://doi.org/10.1016/j.ceramint.2024.05.317
[19] M. Rasheed, S. Shihab, O. Alabdali, A. Rashid, T. Rashid, Journal of Physics: Conference Series, 1999 (2021) 012077. https://doi.org/10.1088/1742-6596/1999/1/012077
[20] K. K. Khudair, F. Boudou, A. Mohammed, A. Sehmi, A. Belakredar, M. S. Ibrahim, Experimental and Theoretical NANOTECHNOLOGY, 10 (2026) 869. https://doi.org/10.56053/10.S.869
[21] R. Gulotty, M. Castellino, P. Jagdale, A. Tagliaferro, A. A. Balandin, ACS Nano, 7 (2013) 5114. https://doi.org/10.1021/nn400726g
[22] E. Kadri, M. Krichen, R. Mohammed, A. Zouari, K. Khirouni, Optical and Quantum Electronics, 48 (2016) 1. https://doi.org/10.1007/s11082-016-0812-7

[23] P. Zhang, S. Jia, J. Guo, S. Hu, Construction and Building Materials, 369 (2023) 130388. https://doi.org/10.1016/j.conbuildmat.2023.130388
[24] W. Liu, L. Qin, C. Y. Zhao, and S. Ju, The Journal of Physical Chemistry B, 127 (2023) 2267. https://doi.org/10.1021/acs.jpcb.2c08962
[25] Hoda El-Nagar, M. S. Abd El-Sadek, M. Ibrahim, Sahar Elnobi, Scientific Reports, 15 (2025) 30614. https://doi.org/10.1038/s41598-025-14376-3
[26] H. K. Aity, E. Dhahri, M. Rasheed, Ceramics International, 50 (2024) 54666. https://doi.org/10.1016/j.ceramint.2024.10.324
[27] Y. Miao, Q. Chen, Y. Li, D. Zhuo, and R. Wang, Frontiers in Materials, 10 (2023). https://doi.org/10.3389/fmats.2023.1129676
[28] M. S. Ibrahim, T. T. Issa, B. Yaqoob, E. N. Fayyadh, A. Rashid, R. S. Mahmood, Experimental and Theoretical NANOTECHNOLOGY, 10 (2026) 887. https://doi.org/10.56053/10.S.887
[29] Z. S. Ahmed, M. RASHEED, H. S. Ahmed, Experimental and Theoretical NANOTECHNOLOGY, 10 (2026) 329. https://doi.org/10.56053/10.s.329
[30] Z. S. Ahmed, M. RASHEED, H. S. Ahmed, Experimental and Theoretical NANOTECHNOLOGY, 10 (2026) 343. https://doi.org/10.56053/10.s.343
[31] E. Arif, R. Jamal, M. RASHEED, Experimental and Theoretical NANOTECHNOLOGY, 10 (2026) 453. https://doi.org/10.56053/10.2.453
[32] G. E. Alkinani, A. R. J. Katae, M. RASHEED, Experimental and Theoretical NANOTECHNOLOGY, 10 (2026) 1027. https://doi.org/10.56053/10.S.1027
[33] A. Keziz, M. Rasheed, M. Heraiz, F. Sahnoune, A. Latif, Ceramics International, 49 (2023) 37423. https://doi.org/10.1016/j.ceramint.2023.09.068
[34] M. Laspalas, Agustín Chiminelli, C. Saenz, F. Serrano, and C. Valero, MATEC Web of Conferences, 188 (2018) 01018. https://doi.org/10.1051/matecconf/201818801018
[35] A. A. Hateef, E. Dhahri, M. Rasheed, H. Kadhim, Z. Abbas, N. Hassan, Physics and Chemistry of Solid State, 25 (2024) 801. https://doi.org/10.15330/pcss.25.4.801-810
[36] T. Saidani, S. Mokhtari, M. Rasheed, H. Lahmar, M. Trari, Journal of the Indian Chemical Society, 103 (2026) 102499. https://doi.org/10.1016/j.jics.2026.102499
[37] A. J. Hussein, M. N. Al-Darraji, M. Rasheed, IOP Conference Series: Earth and Environmental Science, 1262 (2023) 022007. https://doi.org/10.1088/1755-1315/1262/2/022007
[38] T. Rashid, M. M. Mokji, M. Rasheed, Journal of Optics, 53 (2024) 1. https://doi.org/10.1007/s12596-024-02080-w
[39] A. A. Abdulrahman, M. Rasheed, S. Shihab, Journal of Physics: Conference Series, 1879 (2021) 022118. https://doi.org/10.1088/1742-6596/1879/2/022118
[40] T. Rashid, M. M. Mokji, M. Rasheed, Journal of the Mechanical Behavior of Materials, 34 (2025) 1. https://doi.org/10.1515/jmbm-2025-0074
[41] M. Enneffati, M. Rasheed, B. Louati, K. Guidara, R. Barillé, Optical and Quantum Electronics, 51 (2019) 1. https://doi.org/10.1007/s11082-019-2015-5
[42] A. Jaber, M. Ismael, T. Rashid, M. A. Sarhan, M. Rasheed, I. M. Sala, Eureka: Physics and Engineering, 4 (2023) 29. https://doi.org/10.21303/2461-4262.2023.002770
[43] A. J. Hussein, M. N. Al-Darraji, M. Rasheed, M. A. Sarhan, IOP Conference Series: Earth and Environmental Science, 1262 (2023) 022005. https://doi.org/10.1088/1755-1315/1262/2/022005
[44] M. Rasheed, I. Alshalal, A. A. Rashed, M. A. Sarhan, A. S. Jaber, Indonesian Journal of Electrical Engineering and Computer Science, 33 (2024) 653. https://doi.org/10.11591/ijeecs.v33.i1.pp653-660
[45] M. Rasheed, M. N. Mohammedali, F. A. Sadiq, M. A. Sarhan, T. Saidani, Journal of Optics, 54 (2024) 1. https://doi.org/10.1007/s12596-024-01928-5
[46] A. R. J. Katae, H. H. Hussein, A. S. Jaber, M. A. Sarhan, M. RASHEED, Experimental and Theoretical NANOTECHNOLOGY, 10 (2026) 795. https://doi.org/10.56053/10.2.795

[47] A. R. J. Katae, H. H. Hussein, A. S. Jaber, M. A. Sarhan, M. RASHEED, Experimental and Theoretical NANOTECHNOLOGY, 10 (2026) 725. https://doi.org/10.56053/10.2.725
[48] H. M. I. Al-Zuhairi, I. Alshalal, H. H. Abbood, M. Al Nuaimi, Experimental and Theoretical NANOTECHNOLOGY, 10 (2026) 855. https://doi.org/10.56053/10.S.855
[49] H. M. I. Al-Zuhairi, I. Alshalal, H. H. Abbood, M. Al Nuaimi, Experimental and Theoretical NANOTECHNOLOGY, 10 (2026) 1093. https://doi.org/10.56053/10.S.1093
[50] W. Saidi, N. Hfaidh, M. Rasheed, M. Girtan, A. Megriche, M. El Maaoui, RSC Advances, 6 (2016) 68819. https://doi.org/10.1039/c6ra15060h
[51] A. Zubaidi, L. M. Asaad, I. Alshalal, M. Rasheed, Journal of the Mechanical Behavior of Materials, 32 (2023) 1. https://doi.org/10.1515/jmbm-2022-0302
[52] M. Enneffati, B. Louati, K. Guidara, M. Rasheed, R. Barillé, Journal of Materials Science: Materials in Electronics, 29 (2018) 171. https://doi.org/10.1007/s10854-017-7901-7
[53] F. Dkhilalli, S. Megdiche, K. Guidara, M. Rasheed, R. Barillé, M. Megdiche, Ionics, 24 (2018) 169. https://doi.org/10.1007/s11581-017-2193-8
[54] F. Boudou, A. Guendouzi, A. Belakredar, M. RASHEED, Notulae Scientia Biologicae, 16 (2024) 13837. https://doi.org/10.55779/nsb16211837
[55] F. Boudou, A. Belakredar, A. Berkane, M. RASHEED, Notulae Scientia Biologicae, 17 (2025) 12183. https://doi.org/10.55779/nsb17212183
[56] A. Aukštuolis, et al., Proceedings of the Romanian Academy Series A: Mathematics, Physics, Technical Sciences, Information Science, 18 (2017) 34. https://hal.archives-ouvertes.fr/hal-02443179
[57] T. Saidani, M. Zaabat, M. S. Aida, R. Barillé, M. Rasheed, Y. Almohamed, Journal of Materials Science: Materials in Electronics, 28 (2017) 9252. https://doi.org/10.1007/s10854-017-6660-9
[58] N. N. Etuk, A. P. I. Popoola, O. M. Popoola, U. O. Uyor, and V. E. Ogbonna, Polymer Nanocomposites, 1 (2026) 89. https://doi.org/10.1016/b978-0-443-13756-3.00017-8
[59] M. Sabet and S. Sabet, Polymer-Plastics Technology and Materials, 64 (2025) 1282. https://doi.org/10.1080/25740881.2025.2460206
[60] M. C. Paiva, B. Zhou, K. A. S. Fernando, Y. Lin, J. M. Kennedy, Y.-P. . Sun, Carbon, 42 (2004) 2849. https://doi.org/10.1016/j.carbon.2004.06.031